Increased mid-infrared supercontinuum bandwidth and average power by tapering large-mode-area chalcogenide photonic crystal fibers

Petersen, Christian Rosenberg; Engelsholm, Rasmus Dybbro; Markos, Christos; Brilland, Laurent; Caillaud, Celine; Troles, Johann; Bang, Ole

Published in:
Optics Express

Link to article, DOI:
10.1364/OE.25.015336

Publication date:
2017

Document Version
Publisher's PDF, also known as Version of record

Research Article | Vol. 25, No. 13 | 26 Jun 2017 | OPTICS EXPRESS 15336
Optics EXPRESS

Increased mid-infrared supercontinuum bandwidth and average power by tapering large-mode-area chalcogenide photonic crystal fibers

CHRISTIAN ROSENBERG PETERSEN,[1,*] RASMUS D. ENGELSHOLM,[1] CHRISTOS MARKOS,[1] LAURENT BRILLAND,[2] CÉLINE CAILLAUD,[2] JOHANN TROLÈS,[3] AND OLE BANG[1,4]

[1]*Department of Photonics Engineering, Technical University of Denmark, DK-2800 Kgs. Lyngby, Denmark*
[2]*SelenOptics, 263 Avenue du Gal Leclerc, Campus de Beaulieu, 35700 Rennes, France*
[3]*Glasses and Ceramics Group, ISCR UMR-CNRS 6226, University of Rennes 1, 35042 Rennes Cedex, France*
[4]*NKT Photonics A/S, Blokken 84, DK-3460 Birkerød, Denmark*
[*]*chru@fotonik.dtu.dk*

Abstract: The trade-off between the spectral bandwidth and average output power from chalcogenide fiber-based mid-infrared supercontinuum sources is one of the major challenges towards practical application of the technology. In this paper we address this challenge through tapering of large-mode-area chalcogenide photonic crystal fibers. Compared to previously reported step-index fiber tapers the photonic crystal fiber structure ensures single-mode propagation, which improves the beam quality and reduces losses in the taper due to higher-order mode stripping. By pumping the tapered fibers at 4 μm using a MHz optical parametric generation source, and choosing an appropriate length of the untapered fiber segments, the output could be tailored for either the broadest bandwidth from 1 to 11.5 μm with 35.4 mW average output power, or the highest output power of 57.3 mW covering a spectrum from 1 to 8 μm.

OCIS codes: (320.6629) Supercontinuum generation; (190.4370) Nonlinear optics, fibers; (060.2390) Fiber optics, infrared.

References and links

1. B. Bureau, C. Boussard, S. Cui, R. Chahal, M. Anne, V. Nazabal, O. Sire, O. Loréal, P. Lucas, V. Monbet, J.-L. Doualan, P. Camy, H. Tariel, F. Charpentier, L. Quetel, J.-L. Adam, and J. Lucas, "Chalcogenide optical fibers for mid-infrared sensing," Opt. Eng. **53**(2), 027101 (2014).
2. B. Zhang, C. Zhai, S. Qi, W. Guo, Z. Yang, A. Yang, X. Gai, Y. Yu, R. Wang, D. Tang, G. Tao, and B. Luther-Davies, "High-resolution chalcogenide fiber bundles for infrared imaging," Opt. Lett. **40**(19), 4384–4387 (2015).
3. G. S. Athanasiou, J. Ernst, D. Furniss, T. M. Benson, J. Chauhan, J. Middleton, C. Parmenter, M. Fay, N. Neate, V. Shiryaev, M. F. Churbanov, and A. B. Seddon, "Toward mid-infrared, subdiffraction, spectral-mapping of human cells and tissue: SNIM (Scanning near-field infrared microscopy) tip fabrication," J. Lightwave Technol. **34**(4), 1212–1219 (2016).
4. A. B. Seddon, "A prospective for new mid-infrared medical endoscopy using chalcogenide glasses," Int. J. Appl. Glass Sci. **2**(3), 177–191 (2011).
5. C. R. Petersen, U. Møller, I. Kubat, B. Zhou, S. Dupont, J. Ramsay, T. Benson, S. Sujecki, N. Abdel-Moneim, Z. Tang, D. Furniss, A. Seddon, and O. Bang, "Mid-infrared supercontinuum covering the 1.4–13.3 μm molecular fingerprint region using ultra-high NA chalcogenide step-index fibre," Nat. Photonics **8**(11), 830–834 (2014).
6. T. Cheng, K. Nagasaka, T. H. Tuan, X. Xue, M. Matsumoto, H. Tezuka, T. Suzuki, and Y. Ohishi, "Mid-infrared supercontinuum generation spanning 2.0 to 15.1 μm in a chalcogenide step-index fiber," Opt. Lett. **41**(9), 2117–2120 (2016).
7. R. Gattass, L. Shaw, V. Nguyen, P. Pureza, I. Aggarwal, and J. Sanghera, "All-fiber chalcogenide-based mid-infrared supercontinuum source," Opt. Fiber Technol. **18**(5), 345–348 (2012).
8. S. Kedenburg, T. Steinle, F. Mörz, A. Steinmann, and H. Giessen, "High-power mid-infrared high repetition-rate supercontinuum source based on a chalcogenide step-index fiber," Opt. Lett. **40**(11), 2668–2671 (2015).

#295542 https://doi.org/10.1364/OE.25.015336
Journal © 2017 Received 9 May 2017; revised 10 Jun 2017; accepted 12 Jun 2017; published 22 Jun 2017

Optics EXPRESS

9. M. Michalska, J. Mikolajczyk, J. Wojtas, and J. Swiderski, "Mid-infrared, super-flat, supercontinuum generation covering the 2-5 μm spectral band using a fluoroindate fibre pumped with picosecond pulses," Sci. Rep. **6**(1), 39138 (2016).
10. B. Zhang, Y. Yu, C. Zhai, S. Qi, Y. Wang, A. Yang, X. Gai, R. Wang, Z. Yang, and B. Luther-Davies, "High brightness 2.2-12 μm mid-infrared supercontinuum generation in a nontoxic chalcogenide step-index fiber," J. Am. Ceram. Soc. **99**(8), 2565–2568 (2016).
11. T. A. Birks, W. J. Wadsworth, and P. S. Russell, "Supercontinuum generation in tapered fibers," Opt. Lett. **25**(19), 1415–1417 (2000).
12. S. Shabahang, G. Tao, M. Marquez, H. Hu, T. Ensley, P. Delfyett, and A. Abouraddy, "Nonlinear characterization of robust multimaterial chalcogenide nanotapers for infrared supercontinuum generation," J. Opt. Soc. Am. B **31**(3), 450–457 (2014).
13. A. Marandi, C. W. Rudy, V. G. Plotnichenko, E. M. Dianov, K. L. Vodopyanov, and R. L. Byer, "Mid-infrared supercontinuum generation in tapered chalcogenide fiber for producing octave-spanning frequency comb around 3 μm," Opt. Express **20**(22), 24218–24225 (2012).
14. C. W. Rudy, A. Marandi, K. L. Vodopyanov, and R. L. Byer, "Octave-spanning supercontinuum generation in in situ tapered As_2S_3 fiber pumped by a thulium-doped fiber laser," Opt. Lett. **38**(15), 2865–2868 (2013).
15. D. D. Hudson, S. A. Dekker, E. C. Mägi, A. C. Judge, S. D. Jackson, E. Li, J. S. Sanghera, L. B. Shaw, I. D. Aggarwal, and B. J. Eggleton, "Octave spanning supercontinuum in an As_2S_3 taper using ultralow pump pulse energy," Opt. Lett. **36**(7), 1122–1124 (2011).
16. Y. Sun, S. Dai, P. Zhang, X. Wang, Y. Xu, Z. Liu, F. Chen, Y. Wu, Y. Zhang, R. Wang, and G. Tao, "Fabrication and characterization of multimaterial chalcogenide glass fiber tapers with high numerical apertures," Opt. Express **23**(18), 23472–23483 (2015).
17. Q. Coulombier, L. Brilland, P. Houizot, T. Chartier, T. N. N'guyen, F. Smektala, G. Renversez, A. Monteville, D. Méchin, T. Pain, H. Orain, J. C. Sangleboeuf, and J. Trolès, "Casting method for producing low-loss chalcogenide microstructured optical fibers," Opt. Express **18**(9), 9107–9112 (2010).
18. P. Toupin, L. Brilland, D. Mechin, J.-L. Adam, and J. Troles, "Optical aging of chalcogenide microstructured optical Fibers," J. Lightwave Technol. **32**(13), 2428–2432 (2014).
19. W. Wadsworth, A. Witkowska, S. Leon-Saval, and T. Birks, "Hole inflation and tapering of stock photonic crystal fibres," Opt. Express **13**(17), 6541–6549 (2005).
20. J. Hu, C. Menyuk, L. Shaw, J. Sanghera, and I. Aggarwal, "A mid-IR source with increased bandwidth using tapered chalcogenide photonic crystal fibers," Opt. Commun. **293**, 116–118 (2013).
21. J. Lægsgaard, "Modeling of nonlinear propagation in fiber tapers," J. Opt. Soc. Am. B **29**(11), 3183–3191 (2012).
22. J. Laegsgaard, "Mode profile dispersion in the generalised nonlinear Schrödinger equation," Opt. Express **15**(24), 16110–16123 (2007).
23. M. Kolesik, E. Wright, and J. Moloney, "Simulation of femtosecond pulse propagation in sub-micron diameter tapered fibers," Appl. Phys. B **79**(3), 293–300 (2004).
24. T. Kohoutek, X. Yan, T. Shiosaka, S. Yannopoulos, A. Chrissanthopoulos, T. Suzuki, and Y. Ohishi, "Enhanced Raman gain of Ge–Ga–Sb–S chalcogenide glass for highly nonlinear microstructured optical fibers," J. Opt. Soc. Am. B **28**, 2294 (2011).
25. A. Prasad, C. J. Zha, R.-P. Wang, A. Smith, S. Madden, and B. Luther-Davies, "Properties of GexAsySe1-x-y glasses for all-optical signal processing," Opt. Express **16**(4), 2804–2815 (2008).
26. J. C. Travers and J. R. Taylor, "Soliton trapping of dispersive waves in tapered optical fibers," Opt. Lett. **34**(2), 115–117 (2009).
27. A. Judge, O. Bang, B. Eggleton, B. Kuhlmey, E. Mägi, R. Pant, and C. de Sterke, "Optimization of the soliton self-frequency shift in a tapered photonic crystal fiber," J. Opt. Soc. Am. B **26**(11), 2064–2071 (2009).
28. S. T. Sørensen, U. Møller, C. Larsen, P. M. Moselund, C. Jakobsen, J. Johansen, T. V. Andersen, C. L. Thomsen, and O. Bang, "Deep-blue supercontinnum sources with optimum taper profiles--verification of GAM," Opt. Express **20**(10), 10635–10645 (2012).
29. L. Liu, K. Nagasaka, G. Qin, T. Suzuki, and Y. Ohishi, "Coherence property of mid-infrared supercontinuum generation in tapered chalcogenide fibers with different structures," Appl. Phys. Lett. **108**(1), 011101 (2016).
30. P. Toupin, L. Brilland, J. Troles, and J.-L. Adam, "Small core Ge-As-Se microstructured optical fiber with single-mode propagation and low optical losses," Opt. Mater. Express **2**(10), 1359–1366 (2012).
31. C. Florea, J. Sanghera, L. Busse, B. Shaw, F. Miklos, and I. Aggarwal, "Reduced Fresnel losses in chalcogenide fibers obtained through fiber-end microstructuring," Appl. Opt. **50**(1), 17–21 (2011).
32. C. Markos, "Thermo-tunable hybrid photonic crystal fiber based on solution-processed chalcogenide glass nanolayers," Sci. Rep. **6**(1), 31711 (2016).

1. Introduction

Chalcogenide glass fibers is an excellent medium for nonlinear applications in the mid-infrared (MIR), and offers flexible delivery and collection of broadband MIR light for fiber-based sensing applications, such as: Fiber evanescent wave spectroscopy (FEWS) [1], bundled-fiber imaging [2], scanning fiber near-field spectroscopy [3], and fiber medical

Optics EXPRESS

endoscopy [4]. However, coupling light over a broad bandwidth to a fiber can be challenging and often leads to excessive losses. Especially conventional thermal light sources have very low coupling efficiency due to low spatial coherence, but even highly coherent light sources such as quantum cascade lasers will endure debilitating coupling losses. Consequently, MIR sensing applications would greatly benefit from broadband fiber-based light sources, such as the supercontinuum (SC) light source. In supercontinuum generation (SCG), broadband MIR light is generated within the optical fiber by a pump laser, which allows for robust and portable all-fiber systems, provided that suitable MIR fiber pump lasers are developed. Recent experimental work with SCG has demonstrated spectra spanning more than 11 μm [5,6], covering the entire functional group and a significant part of the fingerprint region of molecular vibrational resonances, thus revealing the true potential of the MIR SC technology. For this reason there has been a rapid development in the community with research groups pursuing both generation of longer wavelengths and higher average output power for enabling applications in the MIR. However, achieving both a long wavelength range and high average power has proved challenging due to the relatively low damage threshold of chalcogenide glasses, and the trade-off between peak power and average power in most available MIR pump systems.

The highest reported supercontinuum output power from a chalcogenide fiber is 565 mW generated in a 10 μm core diameter As_2S_3 step-index fiber (SIF) using a monolithic all-fiber configuration based on cascaded amplification and broadening of a 1.55 μm seed laser emitting 40 ps pulses at a repetition rate of 10 MHz [7]. The spectrum of this source was limited to a maximum wavelength of 4.8 μm due to absorption in the sulphide glass in combination with pumping the fiber in the normal dispersion regime. A similar result with 550 mW output power spanning from 2.8 to 5 μm was achieved by pumping 23 cm of 9 μm core diameter As_2S_3 SIF with ~400 fs pulses at 3.83 μm central wavelength using a free-space optical parametric oscillator (OPO) and amplifier (OPA) system [8]. Although high output power was achieved, neither of these demonstrations provided spectral coverage beyond the current capabilities of fluoroindate fibers, which promise even better power handling than chalcogenides [9]. In comparison, the broadest spectrum spanning from 2 to 15.1 μm was achieved by pumping a 3 cm long 15 μm As_2Se_3 core $AsSe_2$ clad SIF at 9.8 μm with ~170 fs pulses, using a difference frequency generation (DFG) pump scheme based on a 1 kHz Ti:Sapphire oscillator and OPA system [6]. Due to the 1 kHz repetition rate and short pulse duration the maximum achievable output power from such schemes are in the sub mW level [5], and the detection scheme requires sensitive detectors and boxcar/lock-in amplification, which adds to the complexity of the system. More recently an average power of 17 mW over a broad bandwidth up to 11.1 μm at the −30 dB level was demonstrated by pumping a 6 μm core $Ge_{15}Sb_{15}Se_{70}$/$Ge_{20}Se_{80}$ high numerical aperture (NA) SIF with ~330 fs pulses at 4.49 μm using a 21 MHz single-pass OPA system [10]. However, due to the small core diameter very strong focusing of the OPA beam was required, thus reducing the coupling efficiency and the pump power threshold for optical damage to the fiber end-facet.

Almost twenty years ago it was demonstrated that efficient SCG could be obtained with high coupling efficiency by tapering large-core silica SIFs [11]. Subsequently, many have tried to translate this scheme into the MIR using chalcogenide SIFs, but results have been limited to output powers of 3-15 mW covering the 1-5 μm spectral range [12–16]. One issue with tapering chalcogenide SIFs is that any higher-order modes excited in the large-core fiber will be stripped during the down-taper transition. In this paper we demonstrate SCG in tapered large-mode-area $Ge_{10}As_{22}Se_{68}$ photonic crystal fibers (PCF) with record high average output power above 4.5 μm and spectra covering from 1 to 11.5 μm. This was possible because the large mode-area enables high coupling efficiency and damage threshold, while the tapered section enables strong nonlinear interaction and anomalous dispersion at the pump wavelength – all of which improves the efficiency of generating a long-wavelength (LW) continuum. Furthermore, in contrast to SIFs the PCF structure ensures single-mode

Optics EXPRESS

propagation, which improves the beam quality and reduces losses in the taper due to higher-order mode stripping.

2. Fiber and taper characterization

The fibers were fabricated by SelenOptics using a specially developed preform casting method for producing low-loss PCFs from highly purified $Ge_{10}As_{22}Se_{68}$ glass [17]. The drawn fiber has a typical measured baseline loss below 1 dB/m from 3 to 9 μm with signs of impurity absorption from Se-H (4.5-4.7 μm), O-H (2.9 μm), H-O-H (6.3 μm), and Ge-O (7.8 μm) [18], as depicted in Fig. 1(a) for a 12.7 μm core fiber. The fiber transmits up to around 11 μm where the multi-phonon edge of the glass induces significant losses on the order of 10-20 dB/m. Fibers with three different core diameters were produced, and from inspecting the fiber end-facets by confocal microscopy and scanning electron microscopy (SEM) the core diameter (d_{core}), average hole diameter (d), and pitch (Λ) of the structures were accurately determined. An example of this is shown in Fig. 1(c) and the structural dimensions of the fibers used in this study are listed in Table 1. The spontaneous Raman spectrum in Fig. 1(b) was measured in order to calculate the Raman response function for use in numerical modelling. The refractive index of the glass was given only at 1.55 μm to be 2.62, so for modelling of the dispersion and mode properties of the fibers a data set for the similar $Ge_{10}As_{23.4}Se_{66.6}$ glass composition was used [5]. Figure 1(d) shows the calculated dispersion curves for various core diameters assuming a constant pitch-to-hole ratio $d/\Lambda = 0.44$, which is in reasonable agreement with the measured dispersion for the untapered 12.7 μm core diameter fiber.

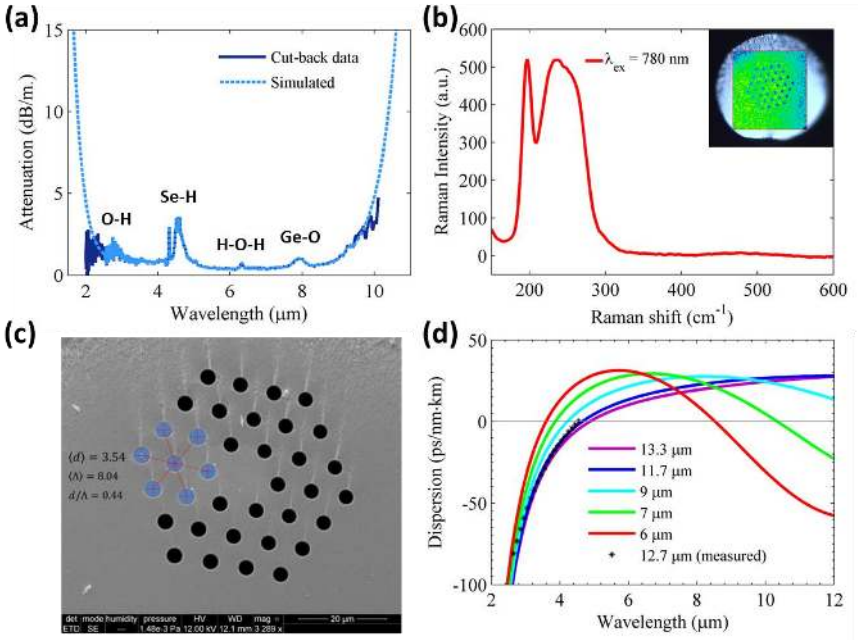

Fig. 1. Characterization of the $Ge_{10}As_{22}Se_{68}$ fiber. (a) Fiber loss in the 12.7 μm core diameter PCF measured using the cut-back technique (solid line), together with the material loss profile used for simulations (dashed). (b) Measured spontaneous Raman scattering spectrum used for modelling the Raman response. Inset shows the collected Raman signal distribution from the fiber end facet (c) SEM image of the fiber end facet showing calculation of the mean hole diameter (d) and pitch (Λ). (d) Calculated dispersion curves for different core diameters assuming constant pitch-to-hole ratio $d/\Lambda = 0.44$ and hole diameter and pitch as in Table 1. The asterisks show the measured dispersion of the 12.7 μm core diameter fiber.

Optics EXPRESS

The figure shows that by tapering down the core diameter as low as 6 μm the first zero-dispersion wavelength (ZDW) can be shifted all the way from 4.8 μm down to 3.6 μm without introducing a second ZDW before 8 μm. Figure 2(a) shows an illustration of a tapered fiber with the different longitudinal sections indicated. The tapers were fabricated post-drawing using a filament-based tapering system operating at 258 °C. The fiber was pulled with a translation speed of 3.8 mm/min, starting tensile strength of 40-50 g, and 15 g in the waist section. The taper was translated with a speed of 4 cm/min to obtain a long uniform waist section. The target length of the waist section (L_W) was 15-20 cm long with 2-3 cm down-taper and up-taper transition regions (L_{DT} and L_{UT}, respectively). Figure 2(e) shows a typical measured down-taper profile. The untapered sections before and after the taper (and L_{AT}, respectively) were initially about 20 cm, making the total length of fiber close to 60 cm. The transmission properties of the long tapered fibers were characterized by Fourier-transform infrared (FTIR) spectrometry, and were found to transmit from 2 to 9.5 μm, as seen from the transmission spectra in Fig. 2(d). The transmission spectrum was heavily influenced by ambient atmospheric absorption from CO_2 at 4.25 μm, and H_2O at 2.9 μm and 5-7.5 μm, respectively. Without fiber end-caps, the open capillaries will over time cause diffusion of water from the air into the glass matrix, which introduces several dBs of loss from impurity absorption at 2.9 μm and 6.3 μm [18]. The LW transmission drop starting from 7.5 μm is believed to be partly due to Ge-O and the multi-phonon absorption edge, but primarily from confinement losses in the taper waist.

To confirm the structural integrity of the fibers after tapering while preserving some fibers for future experiments, three sets of tapers were fabricated and the worst performing taper from each set was then cleaved in the middle of the waist section for inspection. Figure 2(b) and 2(c) show the SEM images (under same magnification) of a tapered 12.7 μm fiber at the input and waist, respectively. The structural parameters for initial and tapered fibers are summarized in Table 1.

Table 1. Mean structural parameters for the produced chalcogenide PCFs measured in the untapered fiber and in the taper waist using SEM and confocal microscopy. The values in parenthesis indicate the diameters of the tapers used for SCG. *: Values estimated from fiber outer diameter (OD).

Initial fiber					Taper waist				
d_{core} [μm]	OD [μm]	d[μm]	Λ[μm]	d/Λ	d_{core} [μm]	OD [μm]	d[μm]	Λ[μm]	d/Λ
11.5	125	3.37	7.57	0.44	6.9	67	1.92	4.46	0.43
12.7	119	3.54	8.04	0.44	8.0 (7.4*)	69 (65)	1.86	5.02	0.37
15.1	176	5.10	10.08	0.51	5.9 (6.1*)	67 (68)	1.89	3.91	0.48

The measurements revealed that while the pitch scales very consistently with the core diameter, the holes contract more than the rest of the structure due to partial hole collapse from the reduced surface tension [19]. From our calculations this partial hole collapse results in both increased confinement loss and a down shift in the dispersion curve, resulting in increasing the first ZDW and lowering of the second ZDW, as shown in Fig. 3. Confinement losses increase in the tapered section because the mode field extends further into the photonic cladding structure, and leakage losses is known to increase even further when the pitch is decreased [20]. The degree of hole collapse was therefore not measured in the actual fibers used for SCG, but assuming a worst case scenario with hole collapse similar to the 12.7 μm fiber, Fig. 3 shows the calculated dispersion and confinement loss with decreasing core diameter for both fibers. It is apparent from the figure that the higher d/Λ results in improved transmission in the long wavelengths, although the fiber may become slightly multi-moded in the short-wavelength (SW) region below 3.5 μm.

Optics EXPRESS

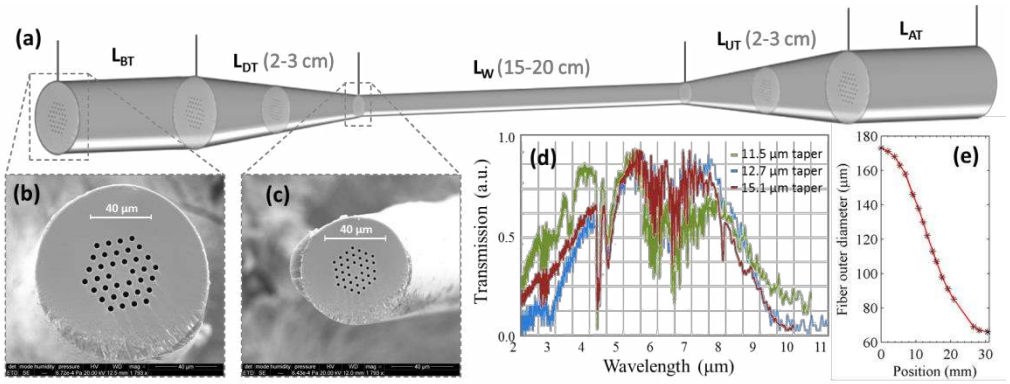

Fig. 2. Taper characterization. (a) Illustration of the longitudinal sections of the tapered fiber: Length before the taper (L_{BT}), down-taper length (L_{DT}), waist length (L_W), up-taper length (L_{UT}), and length after the taper (L_{AT}). (b,c) Same magnification SEM images of the 12.7 µm fiber cross-section in L_{BT} and L_W, respectively. (d) Normalized FTIR transmission through the three tapers before cut-back. (e) Typical measured outer diameter profile in the taper transition region.

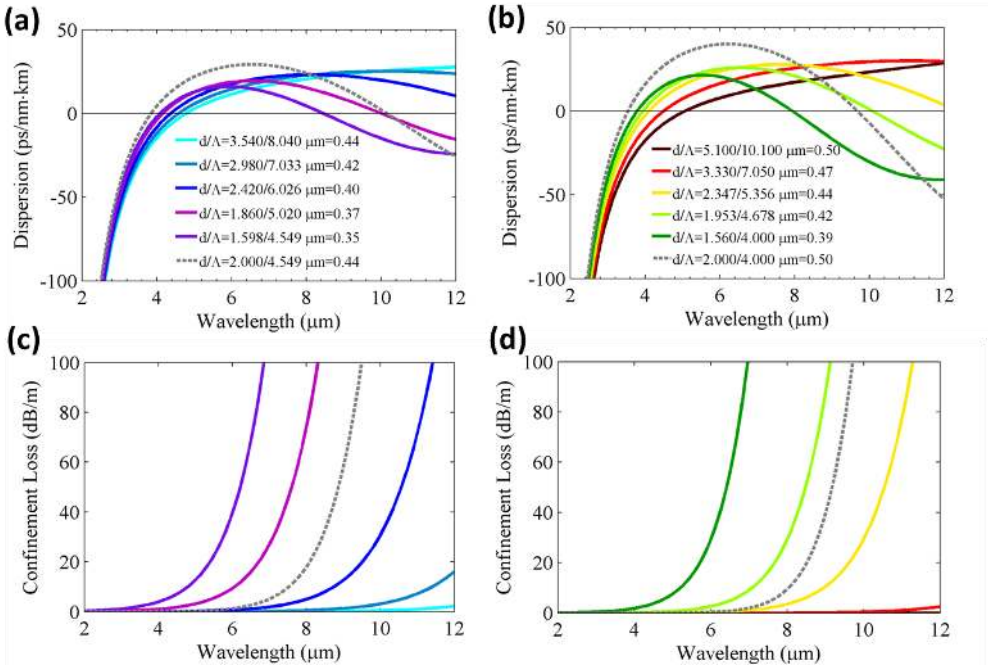

Fig. 3. (a,b) Calculated dispersion and (c,d) confinement losses for the 12.7 µm fiber (a,c) and 15.1 µm fiber (b,d) assuming a linear reduction in hole size (solid lines) as indicated in the legend. The core diameter is given by $2\Lambda - d$. The corresponding dispersion and confinement loss for the smallest core diameter and constant d/Λ is plotted as a dashed line for comparison.

3. Experimental setup for supercontinuum generation

High average power SCG was achieved using the experimental setup shown in Fig. 4. The MIR pump was generated by single-pass parametric generation in a 10 mm periodically-poled fan-out MgO:$LiNbO_3$ crystal (MgO:PPLN). A 1.04 µm mode-locked Yb:KYW solid-state laser was focused inside the crystal together with a CW seed laser in order to stimulate quasi-

Optics EXPRESS

phase-matched parametric anti-Stokes generation. The 1.04 μm laser emitted pulses with a duration of 250 fs at full width half maximum (FWHM) at 21 MHz repetition rate. The seed laser was tunable from 1350 to 1450 nm, which in combination with the variation in poling period over the crystal allowed for a tunable MIR output from around 3.7-4.5 μm. The nonlinear crystal was kept in a heater at a constant temperature of 150°C in order to thermally tune the dispersion to achieve the desired phase matching relations. Any residual pump and other unwanted radiation below 3.5 μm were filtered out using a reflective long-pass filter, and the MIR output beam was subsequently collimated by an achromatic air-spaced lens doublet optimized for 4 μm central wavelength. The output spectrum at 4 μm had a FWHM bandwidth of 93 nm, which corresponds to a 252 fs transform limited Gaussian pulse. The pump beam was coupled into the fibers by a ZnSe aspheric lens with 12 mm focal length, and the pump power was tuned using a wire grid polarizer. The generated continuum was collimated at the output of the fiber using a BD-2 aspheric lens coated for anti-reflection (AR) in the 3-5 μm range, and the spectrum was measured using an FTIR or monochromator-based mercury-cadmium-tellurite (MCT) spectrometer. The output power was measured by a thermal power meter, and long-pass filters with 5% cut-on at 4.5 μm and 6.5 μm with average transmission of ~90% was employed for measuring the LW power.

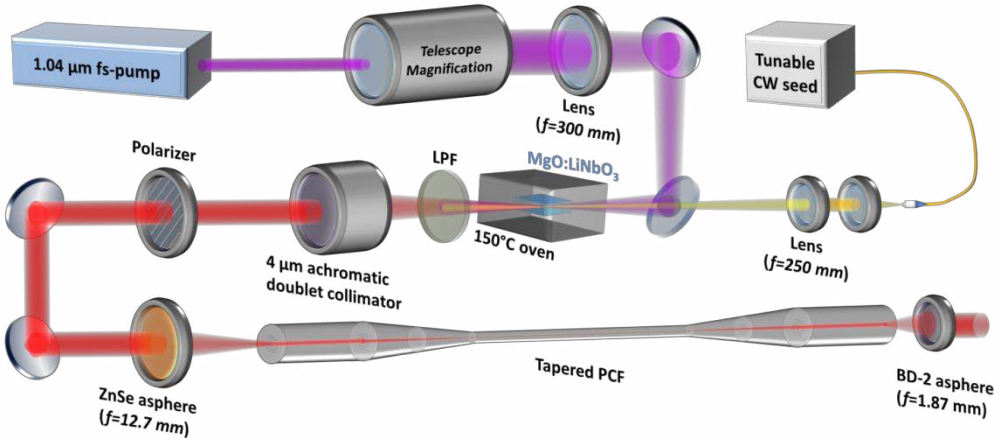

Fig. 4. Experimental setup for MIR pump and supercontinuum generation. A 1.04 μm laser is focused together with a CW seed inside the nonlinear crystal for parametric anti-Stokes generation. The light below 3.5 μm is filtered out and the beam collimated by an achromatic doublet. The beam is directed to a ZnSe asphere for fiber coupling, and the power is tuned by a polarizer (BD-2: Black diamond chalcogenide lens, LPF: Long-pass filter).

4. Results

SCG in an untapered 12.7 μm core PCF was investigated first in order to establish a reference for the tapered fibers. Due to the presence of Se-H and C-O impurity absorption bands, the pump wavelength was limited to below 4.2 μm and near 4.4 μm. Furthermore, the OPA pump generation efficiency was reduced at longer wavelengths due to absorption of the MgO:PPLN crystal, so the best case for high average power was to pump at 4 μm. However, since the ZDW of the untapered fiber was around 4.6 μm, pumping at 4 μm led to very low LW generation efficiency, as is evident from Fig. 5(a). For a pump power of 194.5 mW a total output power of 46.3 mW was obtained, having only around 4.3 mW of the power above 4.5 μm. Pumping at 4.4 μm with a pump power of 131 mW was more efficient, and generated a spectrum spanning from 3 to 7.4 μm (30 dB bandwidth) in 25 cm fiber with a total average output power of 49.5 mW, 10.5 mW > 4.5 μm. The SC spectra are presented in Fig. 5(a).

The experiment was then repeated using a tapered fiber having $L_{BT} = 20$ cm and $L_{AT} = 34$ cm. From the calculated dispersion of Fig. 3(a) the ZDW was expected to be

Optics EXPRESS

around 4 μm. Pumping first at 4.4 μm with 140 mW resulted in a slightly higher LW efficiency than in the straight fiber with 14.3 mW > 4.5 μm out of a total of 32.5 mW, but it did not improve the LW spectral coverage, as can be seen from Fig. 5(b). This was also the case for 4 μm pumping, although the efficiency in this case was greatly improved by the taper. Pumping with ~200 mW, almost the same spectrum was generated having 12.4 mW > 4.5 μm out of a total of 42.0 mW. It is also apparent from Fig. 5(b) that the SW edge of the spectrum was extended beyond the measurement capability of the FTIR used for the first spectral measurements. For this reason all subsequent measurements were carried out using a monochromator-based MCT spectrometer that could measure from 1 to 16 μm.

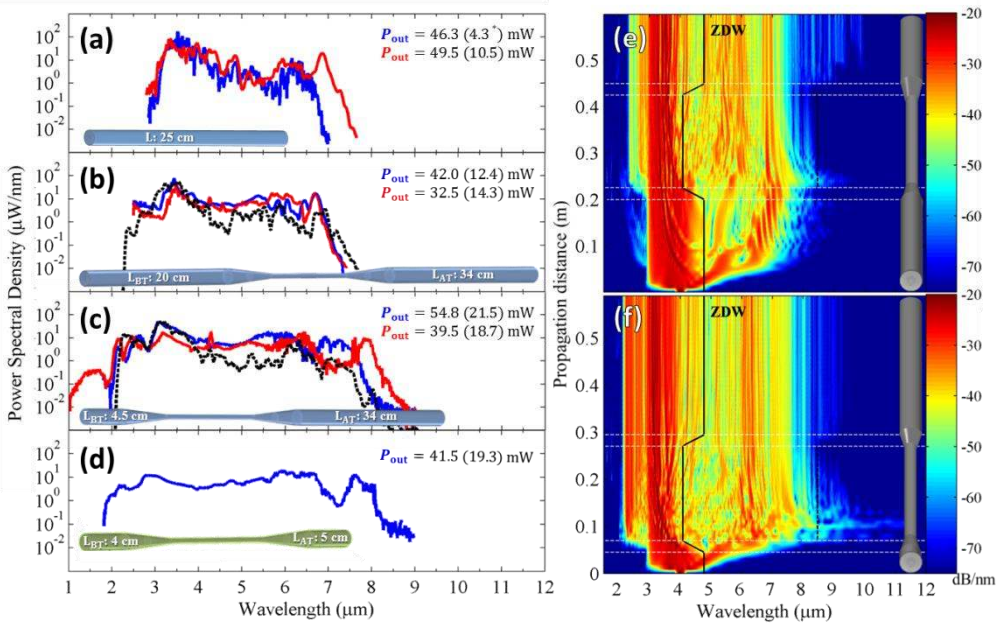

Fig. 5. Overview of experimental results with (a-c) 12.7 μm and (d) 11.5 μm fibers pumping at 4.0 μm (blue) and 4.4 μm (red). (a) SC generated in 25 cm untapered 12.7 μm fiber (*: Power above 4.5 μm was in this case derived from the PSD plot normalized to the total output power). (b,c) Experimental (solid) and numerical (dashed) output spectra for a tapered 12.7 μm fiber with L_{BT} ~ 20 cm and L_{BT} ~ 4.5 cm, respectively. (d) Output spectrum for the 11.5 μm fiber having both a short L_{BT} ~ 4 cm and L_{AT} ~ 5 cm. (e,f) Numerical modelling of experiments with 4 μm pumping in (b) and (c), respectively, showing the effect of the cut-back for a 250 fs Gaussian pulse with 16 kW peak power. The different sections of the taper is indicated by white dashed lines, and the ZDWs are indicated by black lines.

The lack of LW extension from the tapered fiber compared to the straight fiber was attributed to both the high confinement losses in the waist region, but also due to the long length of L_{BT}, which was comparable in length to the untapered fiber from the first experiment. Consequently, the SC is expected to have almost fully developed and dispersed before the down-taper, resulting in lower nonlinear interaction in the waist. To investigate this we cut back the untapered section to 4.5 cm before the down-taper transition and repeated the experiment. The results presented in Fig. 5(c) clearly show the improvement of the LW edge after cut-back. Pumping at 4 μm and 4.4 μm the spectrum now extended from 1.98 to 7.92 μm and 1.95-8.58 μm at the −30 dB level, with an output power of 54.8 mW (21.5mW > 4.5) and 39.5 mW (18.7mW >4.5 μm), respectively. These observations were further supported by SC modelling, as shown in Figs. 5(e)-5(f) for the 4 μm pump case.

In an effort to increase spectral broadening while benefitting from the higher pump power at 4 μm the 11.5 μm fiber with a higher d/Λ=0.43 and smaller waist core diameter d_c = 6.9

Optics EXPRESS

μm was tested. The higher d/Λ and slightly smaller core diameter should result in shifting the ZDW from 4.0 μm to 3.8 μm. To further reduce losses and optimize efficiency the fiber was cut-back in both ends to $L_{BT} = 4\text{cm}$ and $L_{AT} = 5\text{cm}$. Pumping at 4 μm with 231 mW the fiber was able to generate 41.5 mW total average power with 19.3 mW > 4.5 μm, and covering a spectrum up to 8.68 μm. The lower output power suggests high confinement losses at the longer wavelengths and possibly reduced coupling efficiency, so in order to further reduce the effect of confinement loss and increase the coupling efficiency the 15.1 μm core fiber with d/Λ=0.51 was tested. The ZDW in the waist was expected to be between 3.6 and 3.8 μm depending on the actual d/Λ.

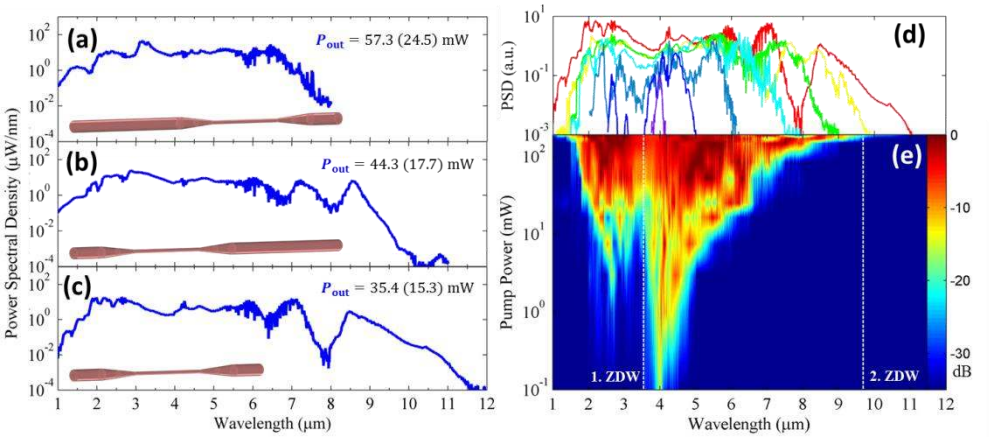

Fig. 6. Overview of experimental results for SC in the 15.1 μm tapered fiber. (a) Highest measured output power with a spectrum from 1 to 8 μm generated with a long L_{BT} ~ 25 cm and short L_{AT} ~ 7.5 cm. (b) SC generated in the same fiber as (a), but coupling in from the other end of the fiber. (c) Broadest SC generated with L_{BT} ~ 7.5 cm and L_{AT} cut back to ~ 4 cm, resulting in extension of the LW edge to 11.5 μm. (d) Output spectra with increasing power for pump case (c). (e) Contour plot illustrating the spectral broadening evolution in pump case (c) with increasing pump power. The dashed lines show the expected ZDWs at the waist assuming negligible hole collapse.

For the 15.1 μm core fiber three different launch configurations were tested on the same fiber: (a) having a long L_{BT} = 25 cm and short L_{AT} = 7.5, (b) opposite configuration so that L_{BT} = 7.5 cm and L_{AT} = 25 cm, and (c) with cutting back the long section to obtain L_{BT} = 4 cm and L_{AT} = 7.5 cm, as shown in Fig. 6(a)-6(c). In the (a) configuration the bandwidth was again limited by the long L_{BT} section. However, surprisingly the resulting bandwidth and output power was very similar to the result in Fig. 5(c) for a short L_{BT}, which suggests that the combination of a larger core, reduced confinement losses, and shorter L_{AT} to some extend countered the effect observed in the first experiment. Having a short L_{BT} section for the (b) configuration resulted in pushing the LW edge further into the MIR, albeit at the expense of output power due to the increased losses at the LWs. Cutting back the L_{AT} section for the (c) configuration should reduce the loss at the LW edge, and consequently the spectrum now extended all the way to 11.5 μm. However, unexpectedly the output power was further reduced after cutback, which suggests an extrinsic loss from the cleave or some contamination/degradation of the output facet between the experiments.

Throughout the experiments the total transmission at low pump power was around 29-32%. We measured the loss of the ZnSe lens at 4 μm to be ~4%, and the collimation lens should have similar transmission in the AR range. The theoretical Fresnel loss due to the high refractive index of n = 2.58 at 4 μm results in a nominal reflection of 19.5%, and assuming about 0.5 dB of fiber propagation loss we arrive at a coupling efficiency of 60.2%. The coupling loss includes mode mismatch, tapering/microdeformation loss, and possibly

Optics EXPRESS

scattering at the output facet. It should be noted that the 2-6 μm AR coating from the collimation lens had high reflection loss below 1.8 μm, but had very good transmission at longer wavelengths. Switching to another lens with AR coating from 7 to 14 μm was found to have negligible effect on the long-wavelength power and produced almost identical spectra. Nevertheless, the output power is expected to increase slightly by replacing the collimation lens with a reflective parabolic mirror, albeit at the expense of more complicated alignment.

5. Discussion and analysis

In order to optimize the taper design it was important to understand the underlying dynamics of SCG in the experiments. For this reason we modelled the nonlinear pulse propagation using a specific implementation of the generalized nonlinear Schrödinger equation (GNLSE) for including tapering and multiple propagation modes, derived from Maxwell's equations using the approach of Lægsgaard [21,22] and Kolesik et al. [23]. The PCF geometry and material refractive index data was imported into the commercial software COMSOL to solve for modes, and the numerical implementation was performed in MATLAB using the built-in GPU libraries for fast calculation of the fast Fourier transform and matrix manipulations of large data structures. The numerical implementation uses the split-step method with a Runge-Kutta-Fehlberg solver on the nonlinear step, as well as adaptive step size. Simulations were carried out using 2^{19} bins with a temporal resolution of 4.63 fs, and step sizes between 5 μm to 60 μm. The Raman response used in the simulations was derived from the measured frequency response in Fig. 1(b), and the fractional response was set to $f_R = 0.03$ [24]. The nonlinear coefficient n_2 was given by the manufacturer to be 8.8×10^{-14} cm^2W^{-1}, which agrees well with values found in the literature [25]. The refractive index data was fitted to a Sellmeier polynomial: $n^2 = 1 + B0 + B1/(1-C1^2\lambda^2) + B2/(1-C2^2\lambda^2) + B3/(1-C3^2\lambda^2)$, from which the following Sellmeier coefficients was extracted: B0 = 2.774, B1 = 2.892, B2 = 0.7320, B3 = 0, C1 = 0.4047 μm, C2 = 38.53 μm, C3 = 0. The simulations presented in Figs. 5(e)-5(f), and Fig. 7 assumes a transform-limited Gaussian pump pulse with a full-width at half maximum duration of 250 fs and a peak power of 16 kW was simulated.

In the untapered 12.7 μm fiber the pump was located in the normal dispersion regime far from the ZDW, so initial SCG was driven mainly by self-phase modulation (SPM). From both numerical and experimental observations it is clear that pumping below the ZDW leads to a large build-up of power in the 3-4 μm region due to SPM, which therefore limits the amount of power that cross the ZDW to generate the LW part of the spectrum. Figure 5(e) shows that after just 2 cm of propagation the spectrum extends beyond the ZDW, which then initiate soliton formation and fission followed by soliton self-frequency shifting (SSFS). These soliton dynamics can be seen from the spectrograms in Figs. 7(a)-7(d), together with the appearance of dispersive waves (DW) on the SW edge of the spectrum.

After 5 cm of propagation the pulse has broadened sufficiently across the ZDW to initiate soliton A formation at the LW edge, with a corresponding DW at the SW edge. After 9 cm soliton A has undergone soliton fission and the ejected solitons proceeds to red-shift from SSFS, while trapping part of the generated DWs [26]. At this point soliton B emerges along with corresponding DWs, which proceeds to similarly undergo soliton fission and SSFS. During this process, however, soliton B continuously consume the lesser solitons left in the wake of soliton A, enhancing its energy and shifting rate compared to that of soliton A. This is apparent after 13 cm of propagation, where the spectrally broader soliton B now overlaps with soliton A causing the interference beating observed in Fig. 5(e). After 20 cm of fiber the SSFS starts to stagnate and soliton C emerges.

In the tapered 12.7 μm fiber with a long L_{BT} we find from the simulation in Fig. 5(e) that the SW edge was extended by DWs, but while the LW edge was initially extended after the down-taper transition, it gradually diminished in the waist to around 7 μm due to confinement loss. To reproduce this effect in the simulations it was necessary to reduce the confinement

Optics EXPRESS

loss in the simulations by a factor of 5, corresponding more or less to the $d/\Lambda = 0.37$ curve in Fig. 3(c), which has a ~27 dB/m confinement loss at 7 μm compared to ~120 dB/m for $d/\Lambda = 0.35$. This factor may account for the uncertainty of the hole size in the waist. Figure 7(e) show how the shift in dispersion in the down-taper results in both red-shifted DWs (R-DW) across the second ZDW, and in new wavelength components generated in the middle of the spectrum. These mid-spectrum components radiate from the soliton clusters A and B, which indicates that these could be either non-resonant radiation shed by the solitons due to rapid changes in dispersion [26], or from four-wave mixing (FWM) enabled by a longer interaction length and introduction of negative dispersion slope and the second ZDW.

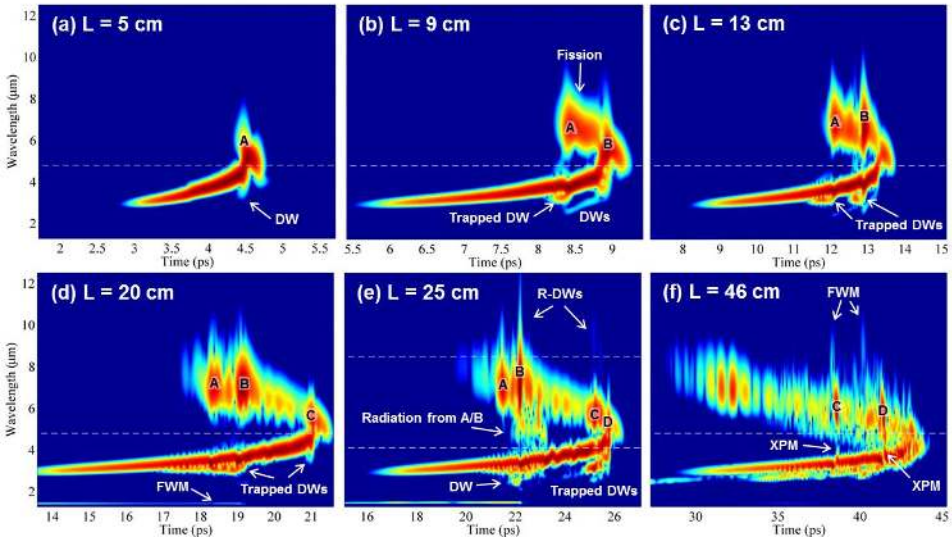

Fig. 7. Simulated time-wavelength spectrograms corresponding to the simulation in Fig. 5(e). (a) Formation of soliton A and DW pair. (b) Fission and red-shift of soliton A, together with emergence of soliton B. (c) Soliton B has merged with lesser solitons and red-shifted beyond soliton A. (d) The SSFS of A and B stagnate, and soliton C emerges just before the down-taper transition. (e) New DWs appear after down-tapering due to change in ZDWs, and energy radiates from soliton clusters A/B. (f) After the up-taper interaction length is again increased, resulting in XPM/FWM between solitons C/D and the SPM-broadened part of the pulse at 3-3.5 μm.

Slightly different dynamics is seen during the up-taper where the changing dispersion causes an enhancement of the interaction between solitons at 6-7 μm and the SPM-broadened main pulse around 3.5 μm, which together with the reduced confinement loss resulted in new spectral components generated at the LW edge from FWM. This effect is seen clearly in Fig. 7(f). The full dynamics can be seen in the supplementary Visualization 1. From these dynamics it is clear, that cutting back the fiber to 4.5 cm before the transition point resulted in capturing more of the pulse in the anomalous dispersion regime and enhancing the SSFS of soliton A before the fission point at ~8 cm [27]. Consequently, the LW generation efficiency was improved, and the SW edge extended. The generation of new spectral components after the up-taper was still observed, although the effect was less pronounced. The full dynamics can be seen in the supplementary Visualization 2.

For the 15.1 μm taper the dynamics was similar, but the greatly improved LW extension indicates that no significant hole collapse occurred during tapering. The high confinement losses expected above 9 μm in the taper waist leads to the conclusion that this part of the spectrum was either generated or amplified during and after the up-taper, where the gradual red-shift of the dispersion lead to increased FWM/XPM interaction, possibly in combination with red-shifted DWs near the second ZDW at 9.7 μm. The continuous SSFS and subsequent

generation of dispersive waves with increasing pump power can be seen from Fig. 6(e), which shows the interpolated spectral development of 11 measurements with increasing pump power and some of the output spectra are shown in Fig. 6(d).

For future optimization we note that it would be advantageous for the LW efficiency to capture as much of the pulse in the anomalous dispersion, which means that the transition should be as close to the input as possible. Furthermore, from simulations we may infer that the results could be improved by having a shorter waist section, since the spectral broadening reaches a maximum shortly after reaching the waist section of the taper, after which the LW edge and output power is continuously diminished by confinement loss. It was also found that a high d/Λ was required for reaching beyond 8.6 μm, so for these reasons it would be advantageous to fabricate a taper with a short L_W and high d/Λ to reduce the confinement losses in the waist. Some length of L_W is still needed in order to favor extension of the LW over the SW, as well as having a short down-taper transition [28,29]. The simulations also indicate that the degree of spectral coherence can be relatively high, but since the calculated coherence is sensitive to the modelled noise, polarization orientation, and actual tapering profile [29] it was not investigated further in this study.

In contrast to previously reported results involving SCG in tapered chalcogenide SIFs [12–14], the PCFs in this work were tapered from a large mode area for improved coupling efficiency, to a moderate waist diameter in order to enable efficient 4 μm pumping, while keeping the confinement loss to a minimum. The advantage of using single-material fibers (i.e. PCFs) compared to high NA SIFs, is that issues with thermo-mechanical compatibility of different glasses during fabrication is avoided, which may alleviate scattering and optical damage associated with inhomogeneities and thermal expansion coefficient mismatch at the core/cladding interface. In this respect the $Ge_{10}As_{22}Se_{68}$ glass composition was chosen over the more nonlinear $As_{40}Se_{60}$ glass due to its stability during fabrication, resistance to crystallization, and higher transition temperature [30], which improves the damage threshold. The obvious disadvantage of using PCFs with air capillaries is the large diffusion surface of the glass, which results in the accumulation of O-H defects from atmospheric water vapor and absorption of the evanescent field. This effect can be avoided by sealing the fiber with a solid endcap immediately after drawing, which has the added benefit of increasing the damage threshold of the fiber and provides the possibility of post-processing the end-facets with anti-reflection coatings or nanoimprinted structures for further improving the output power [31]. Alternatively, the hole structure can be functionalized by integrating chalcogenide nano-layers for further engineering of the thermal and optical properties, providing an extra degree of design flexibility [32].

6. Conclusion

In conclusion we have demonstrated the ability of tapered large-mode-area $Ge_{10}As_{22}Se_{68}$ PCFs to generate broadband MIR SC with record high output power above 4.5 μm. Through testing of tapers with different pitch-to-hole ratio and taper waist diameter the broadest spectra and highest output powers were found to be produced from a 15.1 μm core fiber with the highest initial d/Λ=0.51 tapered down to an estimated 6.7 μm to obtain anomalous dispersion at the 4 μm pump wavelength. By choosing a length of either 4 cm or 24 cm of the untapered fiber before the taper transition the SC output could be optimized for either the broadest bandwidth from 1 to 11.5 μm with 35.4 mW average output power, or the highest output power of 57.3 mW covering a spectrum from 1 to 8 μm, respectively. Based on numerical modelling of the SC dynamics we have proposed several improvements for future optimization, including: shorter waist sections, higher d/Λ, and shorter L_{BT}.

Funding

Danish Council for Independent Research (4184-00359B); Innovation Fund Denmark (4107-00011A); European Commission (FP7-ICT 317803).